A CRISPR-Cas9-based system for the dose-dependent study of DNA double strand breaks sensing and repair

Jocelyn Coiffard, Olivier Santt, Sylvain Kumanski, Benjamin Pardo, María Moriel-Carretero

HAL Id: hal-03418569

https://hal.science/hal-03418569

Preprint submitted on 7 Nov 2021

1

2

3

A CRISPR-Cas9-based system for the dose-dependent study of

DNA double strand breaks sensing and repair

6

Jocelyn Coiffard[1], Olivier Santt[1], Sylvain Kumanski[1],

Benjamin Pardo[2],* and María Moriel-Carretero[1],*

9

10

[1] *Centre de Recherche en Biologie cellulaire de Montpellier (CRBM), Université de Montpellier – Centre National de la Recherche Scientifique, Montpellier, France*

[2] *Institut de Génétique Humaine (IGH), Université de Montpellier – Centre National de la Recherche Scientifique, Montpellier, France*

15

16

17

* Correspondence to **benjamin.pardo@igh.cnrs.fr** (BP)
                  maria.moriel@crbm.cnrs.fr (MMC)

20

21

22

23

24 **Running Title:** A CRISPR-Cas9-based tool to study DSBs dose-dependently

Abstract

The integrity of DNA is put at risk by different lesions, among which double strand breaks (DSBs) occur at low frequency, yet remain one of the most life-threatening harms. The study of DSB repair requests tools provoking their accumulation, and include the use of chemical genotoxins, ionizing radiations or the expression of sequence-specific nucleases. While genotoxins and irradiation allow for dose-dependent studies, nucleases expression permits assessments at precise locations. In this work, we have exploited the repetitiveness of the Ty transposon elements in the genome of *Saccharomyces cerevisiae* and the cutting activity of the RNA-guided Cas9 nuclease to create a tool that combines sequence specificity and dose-dependency. In particular, we can achieve the controlled creation of 0, 1, 15 or 59 cuts in cells with an otherwise identical genetic background. We make the first application of this tool to better understand the behavior of the apical kinase of the DNA damage response Tel1. By comparing different strategies to create DNA breaks, we find that Tel1 is capable of forming multiple foci, in striking contrast with other DSB-related proteins. Tel1 foci are in tight contact with the nuclear periphery, therefore suggesting a role for the nuclear membrane in their congregation.

Introduction

Cells are confronted to an enormous amount of spontaneous DNA damage arising from natural sources, such as reactive oxygen, reactive carbonyl and nitrogen species, products of lipid peroxidation or the spontaneous chemical lability of the DNA. In addition, there are external sources of damage such as ionizing radiations, chemicals in food, air and water as well as ultraviolet light. Last, rare exposure as that occurring during chemotherapy and radiotherapy is intentionally aimed at forming damage to the DNA. The lesions resulting from these attacks are of a heterogeneous nature, and can include nucleotide base opening, adducts, crosslinks and single-stranded DNA breaks. DNA double strand breaks (DSBs) can also occur, albeit in lower proportion, yet remaining one of the most life-threatening lesions (1).

This higher deleteriousness is in great part due to the fact that, contrary to single strand breaks, DSBs more frequently lack an appropriate undamaged, complementary strand to

exploit as a repair template. In fact, DSB repair can efficiently occur without such a support through the process of Non-Homologous End Joining (NHEJ) by sealing the broken ends back together (2). This process could be error-prone because short deletions or insertions may occur at junctions, and translocations take place by the joining between two ends from different DSBs (2). Alternatively, if a sequence similar to the broken one exists elsewhere in the genome, it can be used as a template to guide the information retrieval needed to reconstitute the interrupted sequence at the DSB. This process is Homologous Recombination (HR) and, like NHEJ, is not without drawbacks. The homologous sequence needed to support repair may be available in the replicated sister chromatid or in the homologous chromosome. Further, some sequences are repeated and spread throughout the genome. Given that the resolution of the homology copy may end up with an exchange of the neighboring sequences, a process known as crossing-over, only the repair with the sister chromatid warrants a faithful repair (2).

The study of DSB repair requests tools capable of provoking their accumulation. In this sense, genotoxic agents of chemical nature or different types of ionizing radiations are used to damage the genomes of model organisms in a sequence-unspecific manner. A more controlled strategy relies on the expression of proteins whose enzymatic activity creates DSBs at specific DNA target sequences. These can be endonucleases such as restriction enzymes, commonly used *in vitro* for molecular biology (3–8), and meganucleases known to bear a well-defined, rare sequence only present from once to a few times in a given genome (9–13). For example, much of our understanding about DSB repair mechanisms comes from the analysis of HO-mediated DSB in yeast (11). On the one hand, the use of standard restriction enzymes permits the creation of a relatively high number of breaks, at known positions, with ends of a well-defined structure. On the other hand, the use of specific nucleases cutting at single locations allows to focus the study of molecular events with a high degree of precision while ensuring that no break occurring elsewhere influences the outcome of that DSB event. Yet, a limitation of these sequence-targeted tools is that, contrary to the effects obtained when using increasing doses of genotoxins, they cannot be used for dose-dependent studies. In this sense, in a recent elegant study, Gnügge and Symington engineered a battery of strains in which ß-estradiol addition could trigger the expression of one restriction enzyme at a time, each cutting at an increasing number of sites in the genome, ranging from 20 to 96 (14). However, the different *in vivo* enzymatic activities manifested by each enzyme prevent the use of this system for dose-

86   dependent comparative studies. An alternative work exploited the repetitiveness of the

87   transposable Ty elements in *S. cerevisiae* genome to insert 2, 7 or 11 sites that can be cut upon

88   controlled induction of the HO endonuclease (15). Yet, engineering this system was tedious

89   because it implied multiple rounds of cloning, retrotransposition and Southern blot analysis.

90   This system was used to assess molecular events in DSB repair such as resection and

91   checkpoint activation, as monitored by Southern and western blot, respectively (15,16), and

92   the sensitivity of these techniques allowed to assess dose-dependent differences. Yet, if less

93   sensitive techniques important in the field of DSB sensing and repair need to be used, a system

94   with such a restricted number of breaks may not be sufficient.

95   In this work, we have exploited the repetitiveness of the Ty transposon elements in the

96   genome of *S. cerevisiae* and the guide RNA-driven sequence specificity of Cas9 cutting activity.

97   In particular, we have targeted an increasing number of Ty elements by designing specific

98   guide RNAs (gRNAs) that could recognize one or several Ty classes. Upon the controlled

99   induction of Cas9 expression, we can achieve an increasing number of enzymatic cuts (0, 1, 15

100 or 59) *in vivo*. Because Cas9 and the gRNAs are expressed from plasmids, DSBs can be easily

101 induced in cells grown in otherwise identical conditions and with an identical genetic

102 background. Thus, we have generated a tool that overcomes the lack of dose-dependency of

103 expressing restriction enzymes while achieving the maximum number of DSBs in an easily

104 applicable manner, atypical in systems using sequence-specific nucleases.

105   We applied this tool to assess the behavior of the Tel1 apical kinase of the DNA damage

106 response. Contrary to later-acting factors of the DSB repair cascade, fluorescence microscopy

107 is not commonly used to study the very early-acting factors, especially those involved in DSB

108 sensing. Here, we report that Tel1 molecules congregate in the shape of foci in response to

109 diverse sources of DSBs and we dissect how the kinetics of their formation relate to the DSB

110 dose and to the factors acting downstream. Last, we bring the notion that Tel1 can form up to

111 8 foci per cell, in striking contrast with other DSB-related proteins. Tel1 foci distribute as a ring

112 in tight contact with the nuclear periphery, therefore suggesting a role for the nuclear

113 membrane in their congregation.

114

115

Materials and Methods

Reagents used in this work for cell treatments were zeocin, R25001 ThermoFisher Scientific; camptothecin (CPT), C9911 Sigma-Aldrich; and DAPI, D9542 Sigma-Aldrich.

Culture and treatments: *Saccharomyces cerevisiae* cells carrying plasmids for the expression of the gRNA used to cut the genome and for the expression of the Cas9 endonuclease were grown at 25°C in the appropriate selection medium (-uracil, -leucine). Typically, cells were grown in 2 % glucose; prior to the induction of Cas9 expression, cells were shifted to 2 % glycerol and grown overnight at 25°C to ensure complete glucose consumption. When DNA damage was induced using zeocin (100 µg/mL), cells bearing a control plasmid were grown at 25°C in minimal medium with appropriate selection (uracil). Spot assays were carried out in medium selecting the gRNA plasmids (-uracil) and the inducible Cas9 expression vector (-tryptophan) containing either 2 % glucose or 2 % galactose as a carbon source. Sensitivity spot assays were carried out using YEPD medium supplemented with either DMSO (control) or with 40 µM CPT. For Nup57 tagging with the red fluorophore tDIMER at its genomic *locus*, the plasmid pRS305-*NUP57*-tDIMER (17) (gift from O. Gadal, Toulouse, France) was linearized with *Bgl*II and transformed into strain MM-144. Pus1 was tagged with mCherry using the plasmid YIplac211-mCherry-*PUS1* (18) (a gift from S. Siniossoglou, Cambridge, UK), which was linearized at the *URA3 locus* with *Bgl*II and inserted by HR in this same *locus* in the strain of interest.

Pulsed Field Gel Electrophoresis (PFGE): Agarose plugs containing chromosomal DNA were made as described (19). Chromosomes were separated at 13°C in a 0.9% agarose gel in 0.5× TBE using a Rotaphor apparatus (Biometra) with the following parameters: interval from 100 to 10 s (logarithmic), angle from 120 to 110° (linear), and voltage from 200 to 150 V (logarithmic) during 24 h. The gel was subsequently stained with ethidium bromide for 1 h and washed in water for 30 minutes, then photographed under UV light. For subsequent Southern blot, DNA from gels was transferred to Genescreen Plus membranes

(Perkin Elmer). Hybridization was achieved using multiple radioactive probes specific for the chromosome III (*ARS307 locus*) and chromosome IV (*SLX5, FOB1, RAD9* and *MUS81* genes), and read using a PhosphorImager (Typhoon IP, GE). Three independent biological replicates were performed.

Fluorescence Microscopy: 1 mL of the culture of interest was centrifuged, the supernatant thrown away and the pellet resuspended in the remaining 50 µL. 3 µL of this cell suspension were directly mounted on a microscope slide for immediate imaging of the pertinent fluorophore-tagged protein signals. Imaging was achieved using a Zeiss Axioimager Z2 microscope and visualization, co-localization and analysis done using Image J.

Telomere length measurement: Telomere length was measured by PCR after end labeling with terminal transferase (20,21). End-labeling reactions (40 µL) contained 120 ng genomic DNA, x1 New England Biolabs™ Terminal Transferase Buffer, 1 mM dCTP, 4 units Terminal Transferase (New England Biolabs™) and were carried out at 37°C for 30 minutes followed by heat inactivation at 75°C for 10 minutes. 1/5th volume of 5 M NaCl, 1/80th volume of 1 M $MgCl_2$ and 1 volume of isopropanol were added to the reaction and DNA was precipitated by centrifugation at 17000×g during 15 min. Precipitated DNA was resuspended in 40 µL of ddH_2O. The end-labeled molecules were amplified by PCR using the primer 5'-GCGGATCCGGGGGGGGGGGGGGGGGGG-3' and 5'-TGTGGTGGTGGGATTAGAGTGGTAG-3' (X) and 5'-TTAGGGCTATGTAGAAGTGCTG-3' (Y') , respectively. PCR reactions (50 µL) contained between 40 ng and 80 ng of DNA, 1x myTaq buffer, and primers 0.4 µM each. Amplification was carried out with 5 U of MyTaq polymerase (Meridian Biosciences®). The conditions were 95°C, 5 minutes; followed by 35 cycles of 95°C, 1 minute; 56°C (Y reaction) / 60°C (X reaction), 20 seconds; 72°C, 5 minutes. Reaction was ended with 5 minutes at 72°C. Samples were visualized in a 2 % agarose gel containing 1× GelRed (Ozyme®).

Serial dilution spots assays: Exponentially growing cells of the indicated genotype were serially diluted 10-fold and 3 µL of each dilution spotted onto the indicated plates, incubated for 3 days at 30°C and photographed.

Analysis of DNA content by flow cytometry: 430 µL of culture samples at 10^7 cells/mL were fixed with 1 mL of 100% ethanol. Cells were centrifuged for 1 minute at 16000 xg and resuspended in 500 µL 50 mM Na-Citrate buffer containing 5 µL of RNase A (10 mg/mL, Euromedex, RB0474) and incubated for 2 hours at 50°C. 6 µL of Proteinase K (Euromedex, EU0090-C) were added and after 1 hour at 50°C, cell aggregates were dissociated by sonication (one 3 s-pulse at 50% potency in a Vibracell 72405 Sonicator). 20 µL of this cell suspension were incubated with 200 µL of 50 mM Na-Citrate buffer containing 4 µg/mL Propidium Iodide (FisherScientific). Data were acquired and analyzed on a Novocyte Express (Novocyte).

Quantifications, Graphical Representations and Statistical Analyses: The number of nuclei displaying foci of the analyzed proteins as well as the number of foci present per nucleus were determined visually by the experimenter. Counting was not done in a blinded manner, but three different researchers were implicated in the quantification of experiments to challenge reproducibility. GraphPad Prism was used both to plot the graphs and to statistically analyze the data. The mean value of nuclei displaying foci was calculated for each independent experiment, and the SEM (standard error of the mean) was used to inform on inter-experiment variation. The SEM estimates how far the calculated mean is from the real mean of the sample population, while the SD (standard deviation) informs about the dispersion (variability) of the individual values constituting the population from which the mean was drawn. Given that the goal of our error bars was to describe the uncertainty of the true population mean being represented by the sample mean, we chose to plot the SEM. To plot probability distributions, we converted the actual observations from each category (number of foci) into frequencies by dividing by the total number of observations. To establish the cutting efficiency, band intensities were determined from non-saturated Southern blot

200 images using ImageJ. The signals emanating from cut bands were divided by the addition of

201 signals emanating from both cut and uncut bands, and expressed as a percentage.

202

203 **Strains, plasmids and oligos:** The strains used in this study are presented in

204 Table 1 and were obtained either by classical methods for integration, transformation and

205 crosses, or by CRISPR-Cas9 technology in the case of Tel1 yEGFP-tagging. The plasmids used

206 in this study are presented in Table 2. The relevant sequences for CRISPR-Cas9 manipulations

207 are described in Table 3.

208

209 **Table 1.** Strains used in this study

Simplified Genotype	Full Genotype	Source
WT (W303)	*MAT a, ade2, his3, can1, leu2, trp1, ura3,* GAL+, psi+, *RAD5+*	PP870, Philippe Pasero
tel1Δ	*MAT a, ura3-52, leu2-3,112, his3-i200, trp1-1, trp1-1, lys2-801, tel1ΔKANR*	PP1217, Philippe Pasero
Rad52-YFP Rfa1-CFP mCherry-Pus1	*MAT a, ade2, his3, can1, leu2, trp1, ura3, RAD52-YFP RFA1-CFP mCherry-PUS1::URA3*	PP3558, Philippe Pasero
yEGFP-Tel1 mCherry-Pus1	*MAT a, ade2, his3, can1, leu2, trp1, ura3,* GAL+, psi+, *RAD5+, yEGFP-TEL1, mCherry-PUS1::URA3*	MM-40, this study
yEGFP-Tel1	*MAT a, ade2, his3, can1, leu2, trp1, ura3,* GAL+, psi+, *RAD5+, yEGFP-TEL1*	MM-144, this study
yEGFP-Tel1 Nup57-tDimer	*MAT a, ade2, his3, leu2, trp1, ura3, yEGFP-TEL1 Nup57-tDIMER-RFP::LEU2*	MM-282, this study

210

211 **Table 2.** Plasmids used in this study

Simplified Name	Detailed Information	Source
pEmpty	pRS316	Benjamin Pardo
pMEL10	pMEL10	(22) Addgene #107916
p-*gRNA(x 1 cut)*	pMEL10-gRNA(Ty5)	This study
p-*gRNA(x 15 cuts)*	pMEL10-gRNA(Ty2)	This study
p-*gRNA(x 59 cuts)*	pMEL10-gRNA(Ty2 + Ty1)	This study
p*GALp-CAS9*	pRS415-*GALp-CAS9-CYC1t*	(23) Addgene #43804
p-gRNA(*TEL1p*)	pMEL14-gRNA(*TEL1p*)	This study

p-*TEF1p-CAS9*	pRS414-*TEF1p-CAS9-CYC1t*	(23) Addgene #43802
p-yEGFP	pKT128	(24)
p*NUP57*-tDIMER	pRS305-*NUP57*-tDimerRFP	(17)
p-mCherry-*PUS1*	YIplac211-mCherry-*PUS1*	(18)

212

Table 3. Relevant sequences used in this study (PAM is underlined)

| Simplified name	Sequence	Goal
Ty5 (x 1 cut)	TGTGCAATCACCTGATGATG<u>TGG</u>	Target of gRNA(x 1-cut)
Ty2 *(x 15 cuts)*	GACATTCCTATAAATGCCAT<u>TGG</u>	Target of gRNA(x 15-cuts)
Ty2 & Ty1*(x 59 cuts)*	ATAAGACCTCCACCACATTT<u>AGG</u>	Target of gRNA(x 59-cuts)
TEL1 promoter	AATCAGTGTAACATAGACGA<u>TGG</u>	Target of gRNA(*TEL1*p)
DSBR-Tel1p-fw	CAGGAAATTCGAAAAAAAGCCTTCAAAGAAAA GGGAAATCAGTGTAACATAGACGatgtctaaaggtgaag aattattc	PCR of the repair product to build yEGFP-Tel1
DSBR-Tel1p-rv	ATAGAAAGTTTAAAGTTTCTACAATCCCATGATC CTCCATtaaaccagcaccgtcacctttgtacaattcatccataccatg	PCR of the repair product to build yEGFP-Tel1

214

Results

A genetic system to create DNA double strand breaks in an inducible and dose-dependent manner

In order to generate multiple DSBs, we targeted repeated DNA by using the CRISPR-Cas9 technology (25). Among the most abundant classes of repeats in *S. cerevisiae* are retrotransposons (Ty elements), which represent about 3% of the genome (26), and whose targetability by the CRISPR-Cas9 technology has already been demonstrated in a study aimed at engineering translocations in a controlled manner (27). Based on the sequenced genome of the W303 yeast strain (28), we designed guide RNAs (gRNAs) to target the sole complete Ty5 element (1 cut), the 15 copies of Ty2 (15 cuts) and both the closely related Ty1 and Ty2 (59 cuts) (Fig 1A). The sequences for the gRNAs were cloned in multicopy expression plasmids, different from the one expressing the Cas9 nuclease under the control of the galactose-inducible GalL promoter (22,23).

To assess the performance of the system, we initially tested viability upon inducing Cas9 expression in cells simultaneously expressing no guide RNA (gRNA) and thus no DSB

230 (x 0), or the gRNAs cutting the genome once (x 1), 15 times (x 15) or 59 times (x 59), respectively.

231 By spotting serial dilutions of such cells in medium containing glucose (no Cas9 expression)

232 or galactose (Cas9 expression), we observed that cells simultaneously expressing Cas9 and any

233 gRNA, thus suffering from constant DNA cutting, had difficulties for (x 1 cut) or were

234 incapable of (several cuts) proliferating (Fig 1B, galactose). This genetic evidence suggests that

235 the system is functional.

236
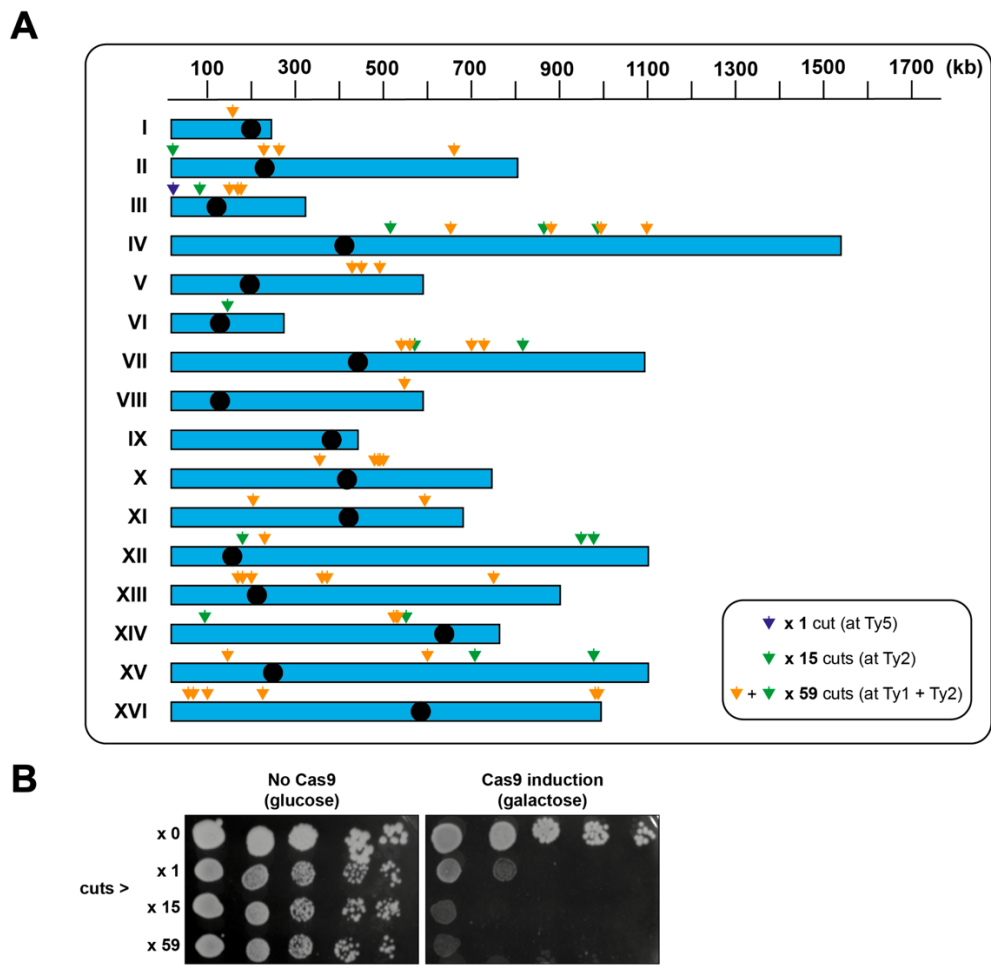
237

238 **Fig 1. Design of the CRISPR-Cas9-based system to induce DSBs in a dose-dependent**

239 **manner**

240 **A.** Scheme of the sixteen *S. cerevisiae* chromosomes (blue boxes), in which the black circles

241 mark the relative position of the centromeres. Color-coded arrows mark the approximate Ty

242 positions targeted by the designed gRNAs. In more detail, the x 1-cut gRNA targets the single

243 Ty5 (dark blue arrow), the x 15-cuts gRNA targets the Ty2 sites (green arrows), and the x 59-

244 cuts gRNA targets both Ty2 and Ty1 sites (orange and green arrows).

B. *S. cerevisiae* WT cells were transformed with the vector bearing an inducible Cas9 and with the vector expressing the relevant gRNA to achieve the desired number of cuts. 10-fold serial dilutions of cells exponentially growing in glucose to prevent Cas9 expression were spotted onto selective minimal medium plates supplemented with the following carbon source: either glucose, to monitor the loading control; or galactose, to induce Cas9 expression.
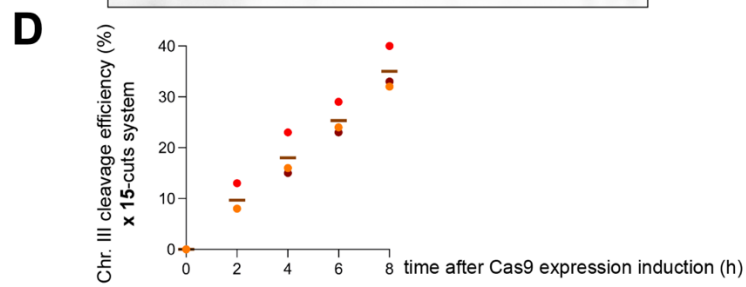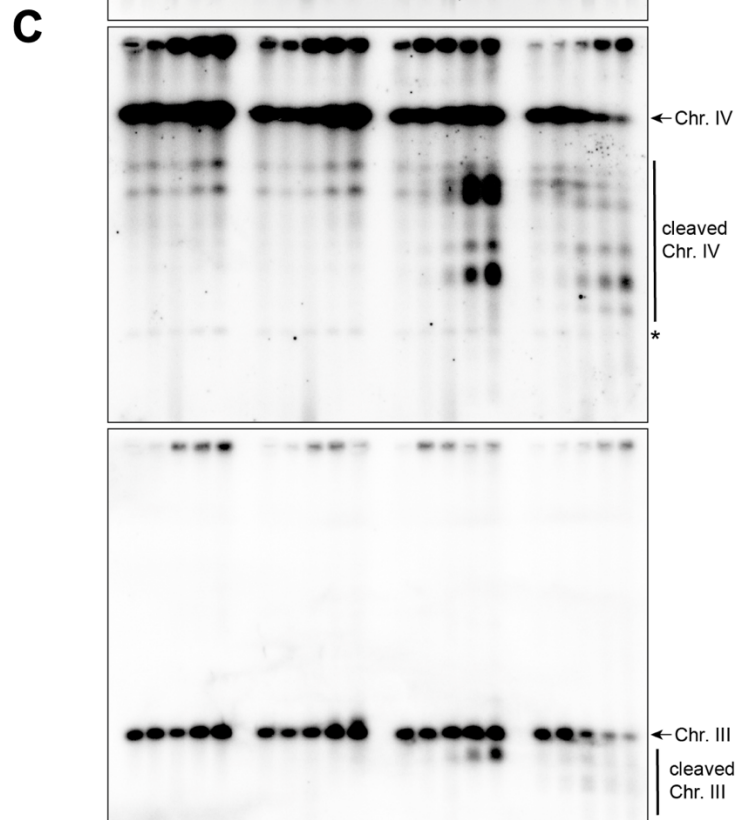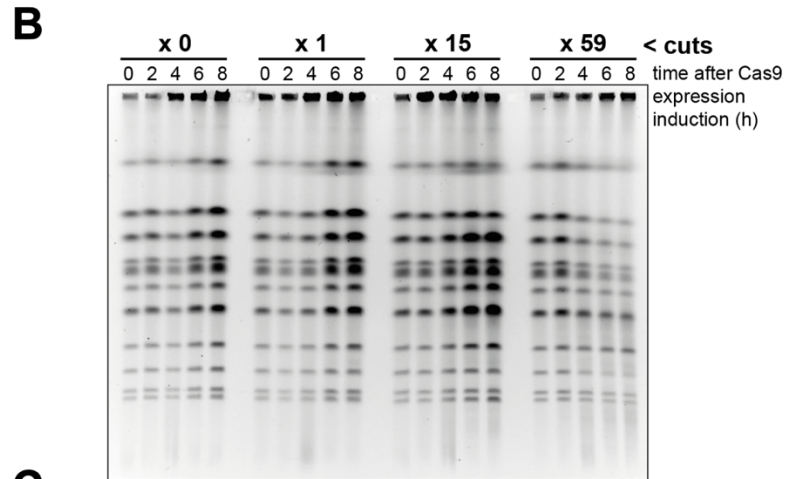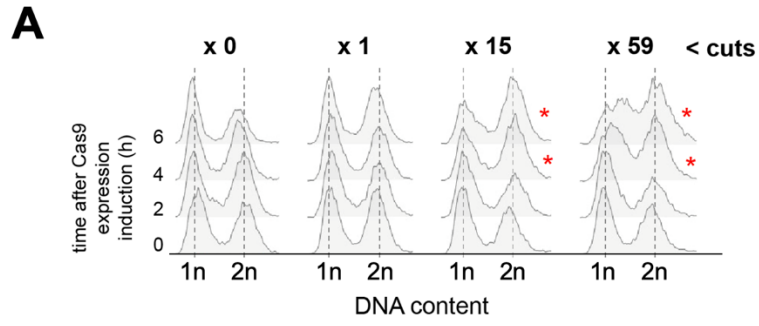
We next wanted to provide a physical and more quantitative characterization of the system. To this end, we grew cells overnight until they reached exponential phase in medium selective for the Cas9 and gRNAs plasmids and with glycerol as the carbon source, allowing a robust and controlled induction of Cas9 upon galactose addition. Cells were recovered and processed for flow cytometry and Pulsed Field Gel Electrophoresis (PFGE) analyses before induction of Cas9 expression and every 2 hours thereafter during 8 hours. The analysis of DNA contents by flow cytometry showed a mild but progressive accumulation of cells in G_2/M in the x 15-cuts and x 59-cuts systems (Fig 2A, red asterisks). These results are consistent with the activation of the DNA damage checkpoint, which halts the cell cycle progression in G_2/M in response to DSBs (29).

Separation of chromosomes by PFGE allows for the detection of broken DNA molecules. No broken DNA molecules could be detected at any of the time-points of the x 0-cut kinetics. However, modest smeared signals were visible in the ethidium bromide-stained gels at late times of the x 15-cuts and x 59-cuts gRNA kinetics (Fig 2B and S1 Fig). Yet, the strongest evidence of molecules being broken emanated from the latest time-points in the x 59-cuts system, when signals corresponding to full chromosomes started to fade away.

To provide formal proof of the breaks, the DNA was transferred and membranes subjected to Southern blot using either a probe directed to the chromosome III or a mix of four probes directed against various locations on chromosome IV. As a result, a time- and dose-dependent pattern of chromosome fragments could be observed (Fig 2C), confirming the proficiency of the system.

A

x 0   x 1   x 15   x 59   < cuts

time after Cas9 expression induction (h)

1n 2n   1n 2n   1n 2n   1n 2n

DNA content

B

x 0   x 1   x 15   x 59   < cuts

0 2 4 6 8   0 2 4 6 8   0 2 4 6 8   0 2 4 6 8   time after Cas9 expression induction (h)

C

←Chr. IV

cleaved Chr. IV

*

←Chr. III

cleaved Chr. III

D

Chr. III cleavage efficiency (%) x **15**-cuts system

time after Cas9 expression induction (h)

273

12

Fig 2. Physical characterization of the DSB-inducible system

A. *S. cerevisiae* WT cells were transformed as in Fig 1B, and a culture of cells growing exponentially in selective minimal medium with glycerol as the carbon source was prepared. A sample was taken at time 0 (before induction). After the addition of galactose, samples were taken at the indicated time points to assess cytometry profiles. n and 2n refer to the DNA content, thus serving as an estimate of the number of cells in G_1 and G_2 phases of the cell cycle, respectively. The red asterisks indicate the time-points at which an increase in the number of cells in G_2/M is detected when compared to the no-cut condition.

B. *S. cerevisiae* WT cells were transformed as in Fig 1B, and a culture of cells growing exponentially in selective minimal medium with glycerol as the carbon source was prepared. A sample was taken at time 0 (before induction). After the addition of galactose, samples were taken at the indicated time points. Cells were processed for Pulsed Field Gel Electrophoresis (PFGE). This technique allows for the separation of chromosomes. The PFGE gel was dyed with ethidium bromide.

C. Southern blot against the DNA from the PFGE shown in **(B)** using one probe targeting chromosome III and four probes targeting chromosome IV. Bands corresponding to full-length chromosomes III and IV are indicated. The asterisk indicates a remaining band corresponding to chromosome III after incomplete stripping of the radioactive probe from the membrane.

D. Quantification of chromosome III cleavage efficiency after Cas9 induction in the x 15-cuts system. The mean values (brown bar) and the individual values (circles) from three independent experiments (indicated by different colours) are plotted for each time point of the time course experiment shown in **(C)**.

We subsequently performed a deep restriction analysis of chromosome cleavage by Cas9 in order to verify the specific cleavages in Ty elements indicated in Fig 1A. We used the known sizes of the full-length chromosome bands from the ethidium bromide-stained gel to infer the sizes of the chromosome fragments that appeared 8h after Cas9 induction on the Southern blot membrane (S1 Fig). In the x 15-cuts system, the chromosome III is expected to be cleaved once, generating a ~254 kb fragment, which we could detect by using a probe targeting this fragment (Fig 3A). We took advantage of this unique cleavage to quantify the cleavage efficiency, which increased progressively to reach a mean value of 35% 8 h after Cas9

induction (Fig 2D). In this same system, 3 cuts are expected in chromosome IV. These cuts can generate various fragments corresponding to the complete or partial cleavage of the chromosome IV (Fig 3A).
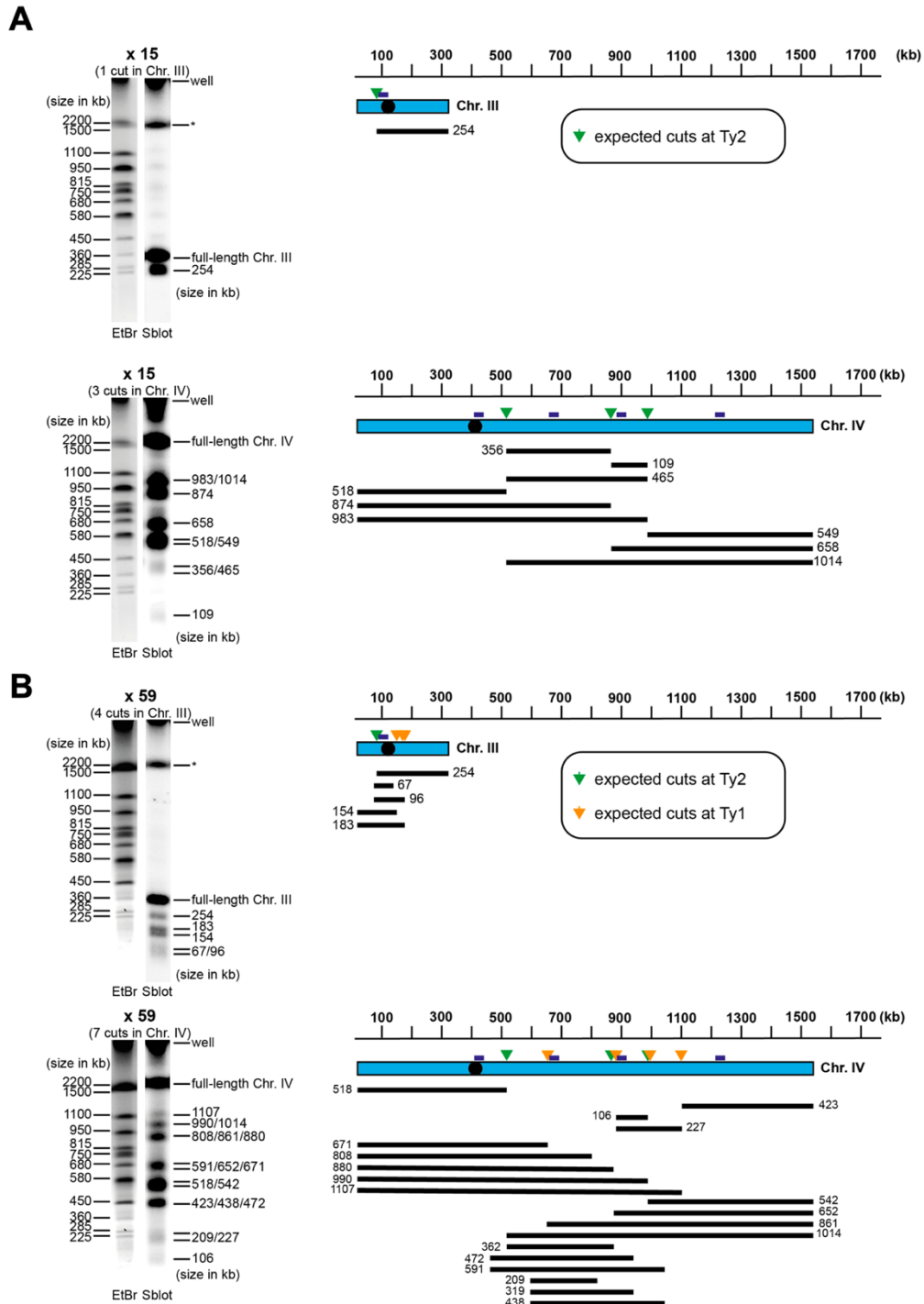
Fig 3. Restriction analyses of chromosome cleavage

A, B. Restriction analysis of chromosomes III and IV cleaved by Cas9 in the x 15-cuts **(A)** and x 59-cuts **(B)** systems. Full-length chromosome sizes (from ethidium bromide-stained gel; EtBr) and inferred fragment sizes (from Southern Blot; Sblot) are indicated in kb. The asterisk indicates a remaining band corresponding to chromosome IV after incomplete stripping of the radioactive probe from the membrane. The approximate Ty positions targeted by the designed gRNAs and the probes used for Southern blot analysis are indicated on chromosome schemes. Restriction patterns are depicted, with expected chromosome fragments sizes, out of both full and partial digestions, indicated in kb. Shown images come from the experiment shown in S1 Fig.

The Southern blot analysis revealed the presence of bands corresponding to all the expected sizes of the chromosome fragments (Fig 3A). We performed the same analysis for the x 59-cuts system, in which four cuts in chromosome III and seven cuts in chromosome IV are expected. We could identify chromosome fragment bands corresponding to all expected restriction patterns thanks to various probes targeting the regions between the cleavage sites (Fig 3B). Overall, we conclude that, albeit with a modest cutting efficiency, our CRISPR-Cas9-based system creates site-specific DSBs in a dose-dependent manner.

**The Cas9-induced DSBs system allows monitoring the dose-dependent kinetics of DNA repair by microscopy**

We exported the system (Cas9 and gRNAs plasmids) to an otherwise WT strain in which early actors of the HR DNA repair pathway were fluorescently tagged. In more detail, the Rfa1 component of the heterotrimeric RPA complex, in charge of binding exposed single stranded DNA (ssDNA), was tagged with CFP at its C-terminus; Rad52, which substitutes RPA for Rad51 on ssDNA to initiate homology search, was tagged with YFP at its C-terminus; and the nucleosoluble protein Pus1 was tagged with mCherry at its N-terminus to clearly define the nucleus. As above, cells were grown overnight to mid-log phase in selective medium plus glycerol, then galactose was added to initiate Cas9 expression. Cells were visualized with the help of a fluorescence microscope and images acquired before Cas9 expression induction and every hour during 7 hours thereafter. We counted the percentage of nuclei in the population displaying Rfa1-CFP and Rad52-YFP foci (at least one focus). The

percentage of nuclei basally displaying Rfa1 foci was of 10 % and fluctuated around this value for each time point when Cas9 was expressed in the absence of any gRNA (Fig 4A,B,D, x 0). Likewise, the lack of DSB maintained a basal level of 4 % of the nuclei displaying Rad52-YFP foci (Fig 4A,C,E, x 0). These data agree with previously reported basal levels for these factors (30), and further confirm that, in the absence of any gRNA, Cas9 alone does not trigger any accumulation of DNA damage. Importantly, the expression of gRNAs driving an increasing number of DSBs permitted us to draw the following observations: First, the system seems to be slightly leaky for, in the absence of Cas9 expression induction, the basal number of Rfa1 and Rad52 foci-forming cells correlatively increased in cells expressing the gRNAs leading to more DSBs (Fig 4B,C). Second, this confirmed the proficiency of the system, since the initial percentage of foci-displaying cells increased with time when the x 1-, x 15- and x 59-cuts gRNAs were present in the cells (Fig 4D,E). Third, the proportion of nuclei displaying Rfa1 foci was consistently double than that of nuclei bearing Rad52 foci, probably reflecting the increased residence time of resected filaments in comparison with the process of homology search (Fig 4C,D). Fourth, and as a general rule, gRNAs driving a higher number of DSBs led to an increased number of cells bearing Rfa1 and Rad52 foci (*i.e.* x15 > x1 > x0), with the higher mean values being of 45% of cells bearing Rfa1 foci and 27% showing Rad52 foci (Fig 4D,E). Surprisingly, from 5 hours onwards, creating 15 DSBs in the genome triggered more Rfa1 foci accumulation than inducing 59 DSBs, and a much faster (although equal in value) accumulation of Rad52 foci (Fig 4D,E, and see discussion). Finally, we observed that increasing numbers of DSBs also increased the number of individual Rfa1 foci per nucleus (S2 Fig). This was not the case for Rad52 foci, which were previously described to be repair centers capable of recruiting more than one DSB (31). Overall, these results suggest that the *bona-fide* DSBs created by our system can be monitored by fluorescence microscopy thus providing insights into the kinetics of DNA repair.
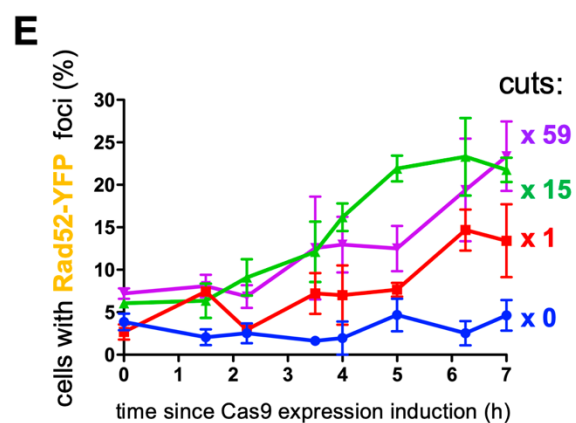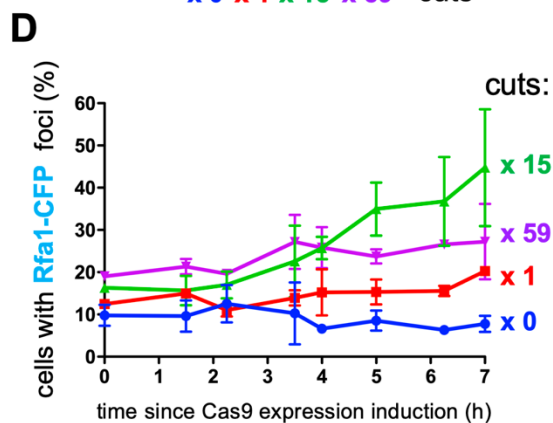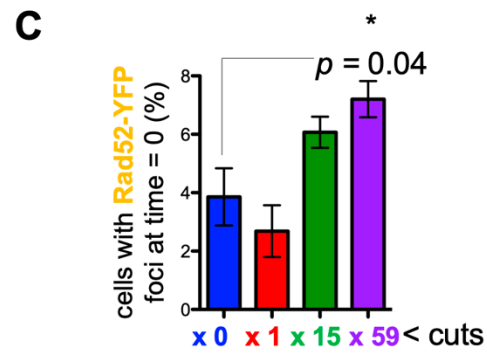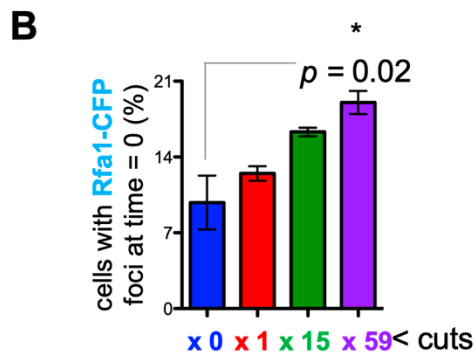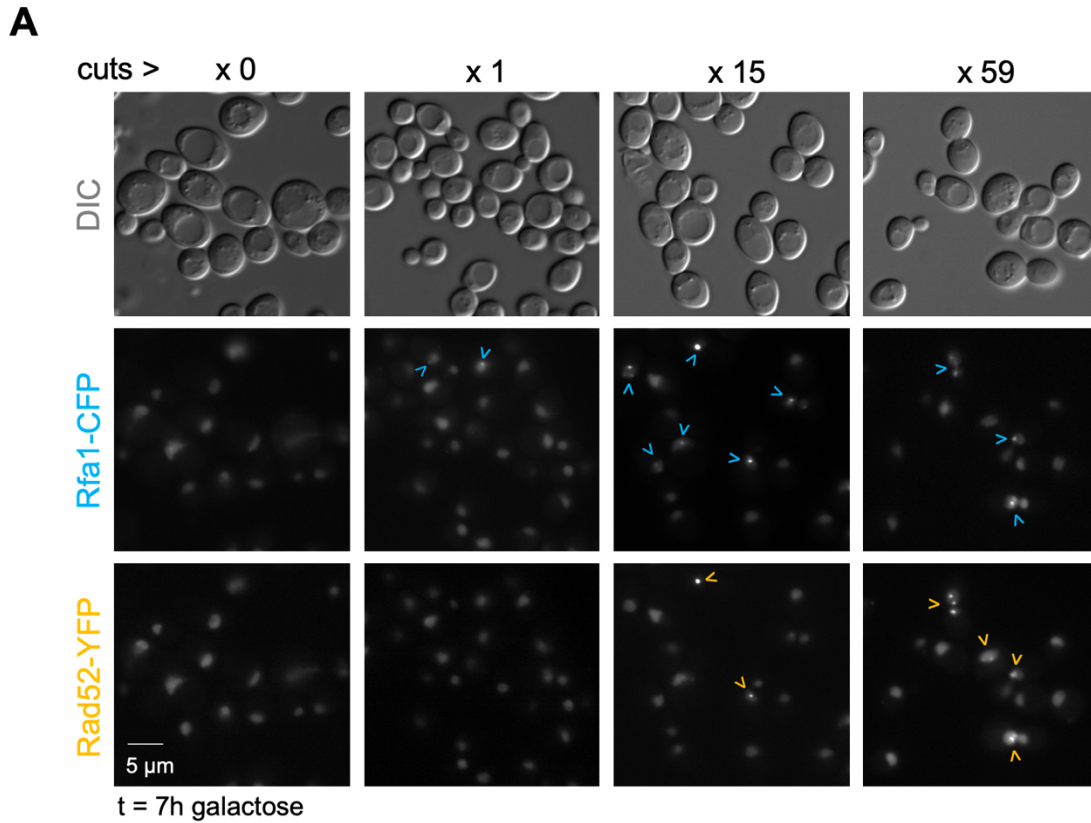
Fig 4. Characterization of DNA repair foci formation in response to increasing Cas9-driven cuts

A. WT cells transformed with the vector expressing an inducible Cas9 and the plasmid expressing the gRNA driving the desired number of cuts grown to exponential phase in

selective minimal medium using glycerol as the carbon source. A sample was taken at time 0 before galactose was added to induce Cas9 expression, samples retrieved at the indicated times, and cells inspected by microscopy. Representative images of Differential Interference Contrast (DIC), Rfa1-CFP and Rad52-YFP channels are shown. Arrowheads point at foci formed by the fluorescently tagged proteins.

B. Percentage of cells in the population displaying at least one focus of Rfa1-CFP in samples from (A) at time 0 (no galactose addition). The bar height is the mean of three independent experiments, and the error bars represent the SEM out of those three experiments. At least 150 cells were considered per condition, time and experiment. The * and the *p*-value indicate the significance of the difference of the means after applying a *t*-test. Each cut scenario is associated with one colour, and this code is maintained in subsequent sections.

C. Percentage of cells in the population displaying at least one focus of Rad52-YFP in samples from **(A)** at time 0 (no galactose addition). Details as in **(B)**.

D. Percentage of cells in the population displaying at least one focus of Rfa1-CFP in samples from **(A)** at different times since galactose addition. Each point is the mean of three independent experiments, and the error bars represent the SEM out of those three experiments.

E. Graph showing the percentage of cells in the population displaying at least one focus of Rad52-YFP in samples from **(A)** at different times after galactose addition. Details as in **(D)**.

Exploiting the dose-dependent DSB system to study Tel1 foci

Fluorophore-tagging of multiple proteins has allowed the establishment of the temporal kinetics from DSB sensing till late steps of its repair (30,32). Yet, compared to the number of works assessing the formation, persistence, dissolution or frequency of foci of DNA repair proteins such as Rad52, the study of very early acting factors such as DSB sensors is under-assessed. DSBs sensing is orchestrated by the early arrival of the MRX (MRN in humans) complex and its immediate binding by the apical kinase of the DNA Damage Response Tel1 (ATM in humans). These foci can form at any stage of the cell cycle, persist if resection is not implemented, as in *SAE2* deletion mutants (30,33) and, in agreement with their early role, do not depend on the ssDNA-coating complex RPA (30). Still, in contrast to Mre11 foci, which have attracted more interest (16,33), Tel1 study by microscopy has been assessed in only one study (30). This little interest may relate to the fact that the absence of Tel1 hardly

sensitizes cells to genotoxic agents, with the exception of Topoisomerase I trapping by camptothecin (CPT) (34), presumably because its deficiency is often compensated by the other apical kinase Mec1 (35,36). Yet, accurate sensing, proper processing and timely checkpoint activation upon DSBs depend on Tel1, and therefore the alternative orchestration by Mec1 may not reflect the physiological pathway that the lesions should have triggered. Moreover, in the event of an increasing number of simultaneous DSBs, Tel1 signaling becomes critical in the absence of Mec1 (16).

We have tagged Tel1 with yeast-enhanced-GFP (yEGFP) at its N-terminus, a location reported to preserve its function (30,37), while conserving its natural promoter. In agreement, strains bearing this modification were as proficient as their isogenic WT in tolerating CPT, as assayed by serial dilution spotting, and in contrast to *tel1Δ* cells (Panel A in S3 Fig). Other than in DSB signaling, Tel1 is key in preserving telomere length, which can be measured by sub-jecting samples to terminal transferase treatment followed by PCR-driven telomere amplifica-tion (20,21). We have monitored both X and Y' telomere length and observed similar sizes in WT and in derived yEGFP-Tel1 cells, in marked contrast with the shorter products observed for *tel1Δ* cells (Panel B in S3 Fig). Thus, we conclude that the fluorescent tag at the N-terminus of Tel1 does not alter its biology and can be used to assess functional questions.

Inducing DSBs with the CRISPR-Cas9 dose-dependent system led to Tel1 forming subnuclear foci (Fig 5A) whose morphology and size did not differ from those reported after DSBs induction with ionizing radiations (30), or other DNA damage-related foci, for example of Rad52 or Rfa1 (Fig 4). Of note, we always observed these foci in the periphery of the nucleus (Fig 5A). Second, the basal level of cells presenting Tel1 foci in the population was low, at around 4% (Fig 5A), suggesting that the basal localization of Tel1 at telomeres does not lead to foci formation. Third, the progressive accumulation of DSBs, dependent on time and on gRNA type, matched a parallel increase in the percentage of cells in the population displaying Tel1 foci (Fig 5A, x 0 < x 1 < x 15 < x 59). In this sense, the maximum obtained value, of 20 % (x 59 cuts at 7 h), was in striking concordance with the percentage of cells displaying Rad52 foci in the same condition (Fig 4E). The concordance was also manifested as a transient advantage in accumulating the foci when 15 DSBs were induced (Fig 5A, x15 at 3h). Concerning the number of Tel1 puncta per nucleus, even after 7 hours of induction of the maximum number of cuts, positive cells rarely displayed more than 1 Tel1 focus (Panel C in S3 Fig). Thus, the N-terminal

tagging of Tel1 by yEGFP represents a performant tool allowing sensitive studies by
microscopy approaches.
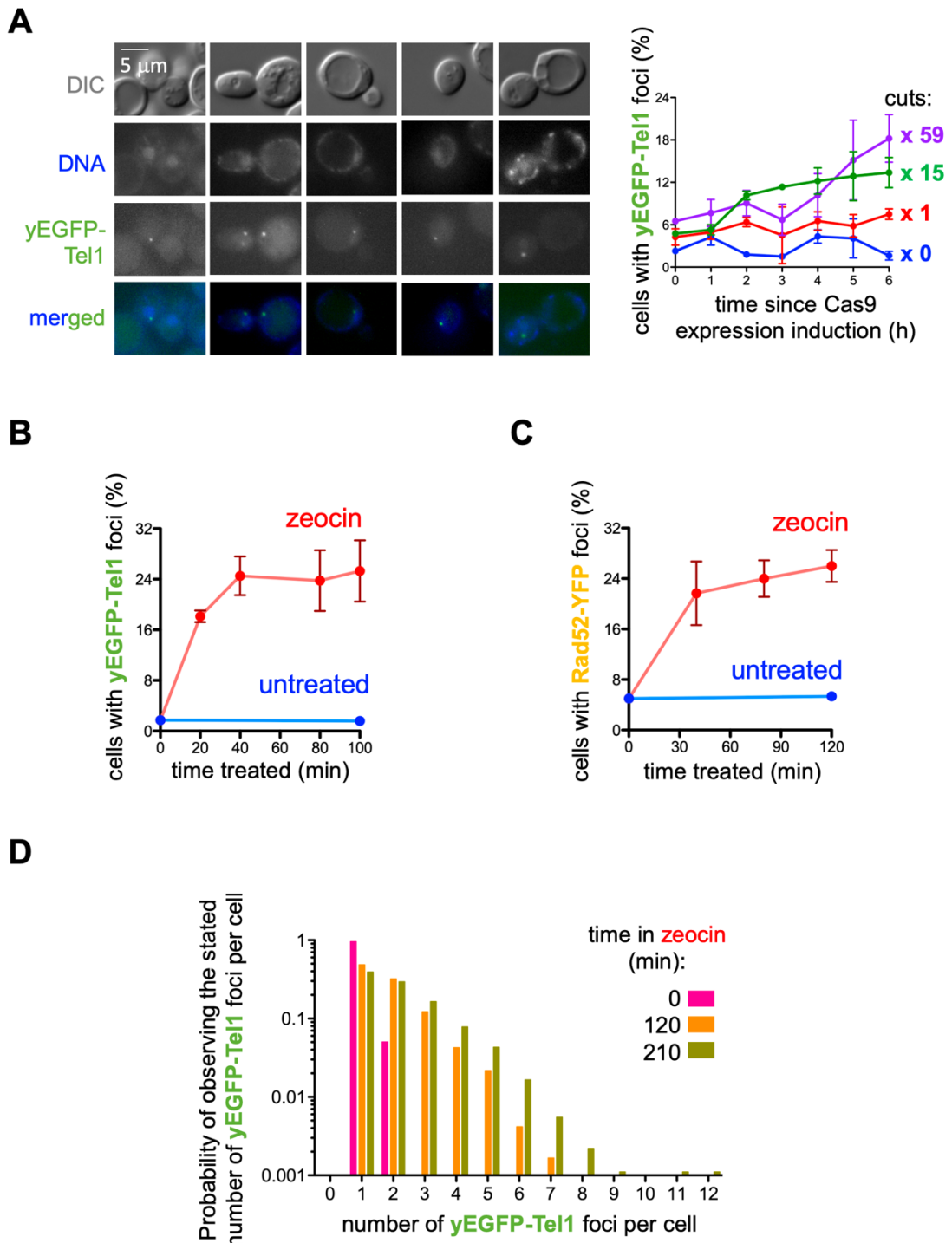
Fig 5. Characterization by microscopy of Tel1 behavior in response to DSBs

A. yEGFP-Tel1 cells transformed with the vector expressing an inducible Cas9 and the plasmid
expressing the gRNA driving the desired number of cuts grown to the exponential phase in

selective minimal medium using glycerol as the carbon source. Samples were taken at time 0 before galactose was added to induce Cas9 expression, and retrieved at the indicated times after induction, and cells inspected by microscopy in search of Tel1 foci. Representative images are shown on the left, for which DNA (both nuclear and mitochondrial) can be visualized with DAPI. The graph on the right shows the percentage of cells in the population displaying at least one focus of yEGFP-Tel1 at different times since galactose addition. Each point is the mean of three independent experiments, and the error bars represent the SEM out of those three experiments. At least 150 cells were considered per time, condition and experiment.

B. An otherwise WT strain tagged with yEGFP at the N-terminus of Tel1 and with mCherry at the N-terminus of Pus1 was transformed with an empty vector allowing its growth in minimal selective medium. Cells were exposed to 100 μg/mL zeocin and samples retrieved for analysis by fluorescence microscopy at the indicated times. The graph shows the percentage of cells in the population displaying at least one focus of yEGFP-Tel1 at different times. Each point is the mean of three independent experiments, and the error bars represent the SEM out of those three experiments. At least 150 cells were considered per time, condition and experiment.

C. Details as in (B) but to score the formation of Rad52-YFP foci.

D. The foci count data obtained from the cells harbouring at least one focus presented in the three experiments described in **(B)** were exploited to build a probability frequency distribution. In brief, the number of Tel1 foci per nucleus was counted and a frequency histogram was drawn. Since the three independent experiments provided similar profiles, all the values were merged to build a more robust distribution. The graph illustrates the probability of finding a nucleus with a given number of Tel1 foci for cells not being exposed to zeocin, or exposed for 120 or for 210 minutes (pink, orange and green bars, respectively).

**Tel1 forms foci at the nuclear membrane upon genotoxin-induced DSBs**

Genotoxins are regularly used to create DNA lesions, among which DSBs. For example, zeocin is reported to trigger the accumulation of DSBs, but also ssDNA breaks (38). Moreover, given the chemical nature of their action, break ends created this way may be heterogeneous, or "dirty". To learn further, we wanted to compare whether chemical induction of DSBs recapitulated Tel1 foci formation upon the induction of DSBs by Cas9. We grew cells in the same conditions as for the Cas9-DSB-inducing system experiments. We acquired images of

473 these untreated cells and then at intervals till 100 min of exposure to 100 μg/mL zeocin. We
474 could observe that Tel1 foci formed at the same frequency in the population as when DSBs
475 were induced by Cas9 (Fig 5B). In more detail, a maximum value of 24 % was reached at 40
476 min that was invariably maintained till 100 min, and monitoring the percentage of cells bearing
477 Rad52-YFP foci demonstrated a strikingly similar kinetics (Fig 5C). Yet, a remarkable
478 difference between Cas9- and zeocin-induced cuts related to the number of Tel1 foci per cell.
479 In fact, we observed that the probability of finding positive cells with more than one (up to 8)
480 Tel1 focus per nucleus increased as time passed by under zeocin treatment (Fig 5D).
481 Interestingly, these Tel1 foci distributed in the shape of a ring, which regularly sat as "a crown
482 on top" of the nucleus (Fig 6A). As such, their subnuclear localization seemed to be mostly
483 peripheral. To consolidate the observation that Tel1 seemed to form in tight proximity to the
484 nuclear envelope, we simultaneously monitored Tel1 foci and the nucleoporin Nup57 marked
485 in its C-terminus with a tDIMER-RFP moiety. In support, Tel1 foci were neatly and recurrently
486 found close to Nup57-tDIMER signals (Fig 6B), with a maximum distance between the
487 maximal intensities of both adjacent signals of 0.3 μm (Fig 6B, right).

488   Overall, we conclude that yEGFP-Tel1 represents an important tool to accurately
489 monitor the very early stages of DSBs signaling, irrespective of whether they are enzymatically
490 or chemically induced. Furthermore, while at the population level the formation of Tel1 foci is
491 perfectly mirrored by the pre-existing tool Rad52-YFP, the subnuclear distribution and
492 congregation patterns of Tel1 foci are different, suggesting the existence of yet unknown
493 aspects of DSBs initial processing.

494
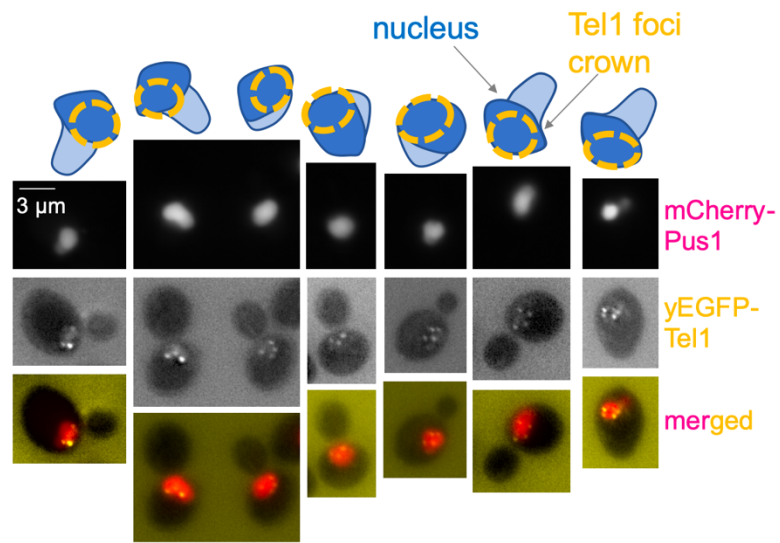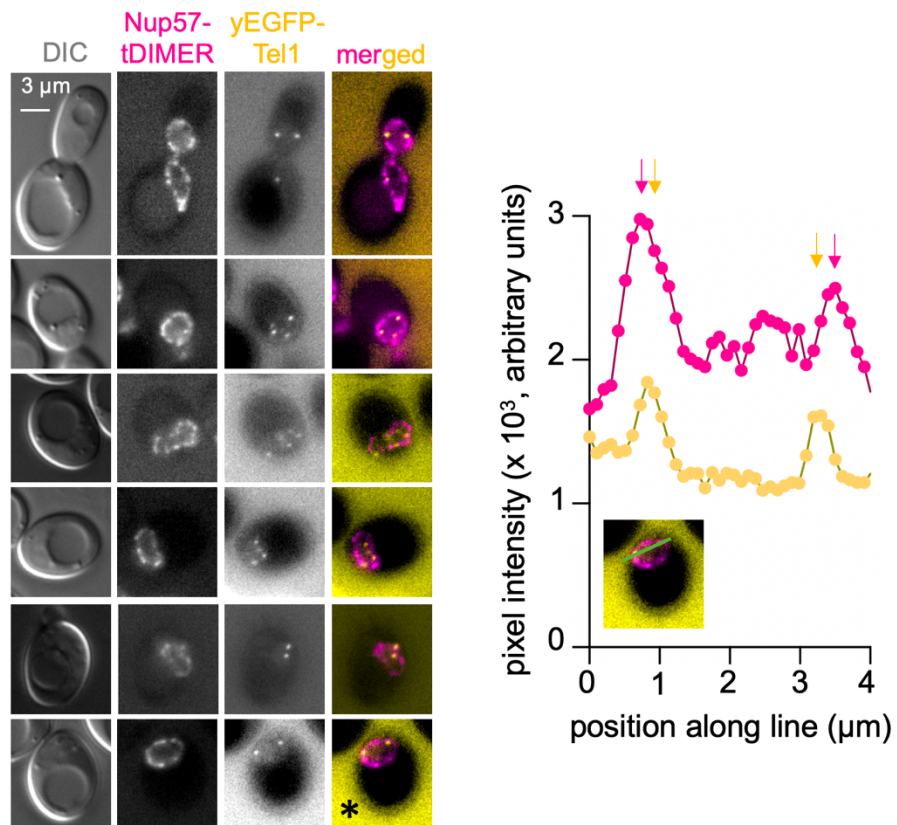
Fig 6. Characterization of the proximity of Tel1 foci to the nuclear membrane

A. An otherwise WT strain was tagged with yEGFP at the N-terminus of Tel1 and with mCherry at the N-terminus of the nucleosoluble protein Pus1 in order to define the nucleoplasm. The subcellular localization of Tel1 was assessed by fluorescence microscopy in response to 100 μg/mL zeocin. Images of both channels as well as their merging are shown.

Since Pus1 signals are slightly less intense in some nuclear regions, notably the nucleolus, this difference is represented by using two different tonalities of blue. Schematic drawings of each imaged nucleus mimic the arrangement of the observed structures to facilitate visualization. **B. Left:** An otherwise WT strain was tagged with yEGFP at the N-terminus of Tel1, and with tDIMER-RFP at the C-terminus of the nucleoporin Nup57 with the goal of defining the nuclear periphery. The relative position of Tel1 foci with respect to nucleoporin signals was assessed by fluorescence microscopy after exposing the cells for 2 h to 100 µg/mL zeocin. Images of the Differential Interference Contrast (DIC), RFP and GFP channels, as well as their merging are shown. The asterisk marks the cell used to create the graph shown on the right. **Right:** A straight line (indicated in green color) was drawn from left to right onto the chosen image and the pixel intensity along it plotted for both the Nup57-tDIMER and yEGFP-Tel1 images. The vertical arrows indicate the points of maximal intensity, thus highlighting the proximity of Tel1 signals to the nuclear periphery.

Discussion

In this work, we have expanded the toolbox in the field of DSB sensing and repair. First, we have taken advantage from the repetitiveness of the transposon elements in the genome of *S. cerevisiae* to design gRNAs capable of driving Cas9 action at specific sites in the genome. Upon Cas9 expression induction, we can compare otherwise identical genomes being broken at an increasing number of locations by the same enzyme. We have validated genetically, physically and functionally the performance of this system. Second, we used this tool to characterize the behavior of the apical kinase of the DNA damage response Tel1. To this end, we used a fluorescent tag at its N-terminus and checked that this did not alter its main known functions in DNA damage sensing and telomere homeostasis. Next, we found that Tel1 molecules congregate in the shape of foci in response to diverse sources of DSB. Furthermore, we show for the first time that Tel1 can form up to 8 foci per cell, distributed in the shape of a crown that seems to be in tight contact with the nuclear periphery.

Previous works have used the repetitiveness of the Ty elements in *S. cerevisiae* genome to insert 2, 7 or 11 restriction sites that can be cut upon controlled induction of the HO endonuclease (15,16). While the design behind our system is reminiscent of this one, we managed to devise a wider range of induced cuts, thus permitting further studies on the dose-

dependency. Indeed, the Ty-HO system was used to assess, by Southern blot, the role of Mre11 on resection as well as, by monitoring the phosphorylation of the downstream effector Rad53, the role of Tel1 in DNA damage signaling (15,16). Given the sensitivity of Southern and western blotting, a maximum of 7 cuts was enough to assess functional differences. Yet, our system provides an enlarged palette of induced DSBs suitable for less sensitive studies. A small drawback of our system was its leakiness: without Cas9 induction, the basal level of Rad52 and of Rfa1 foci increased as a function of the gRNAs used to trigger 1, 15 or 59 cuts, so that the basal number of cuts shown by the strain harboring the 59 DSBs vector doubles that shown by cells without any gRNA (Fig 4B,C). Nevertheless, in spite of this significant basal difference, the window of opportunity for inducing further breaks and characterize them was still wide (Fig 4D,E and S2 Fig).

Tel1 binds DSBs irrespective of the cell cycle phase and, in agreement, Tel1 foci were reported to form at any cell cycle stage, including G_1, in contrast with Rad52 foci, which are mostly S- and G_2-restricted (30). Moreover, break binding by Tel1 occurs before repair is undertaken either by NHEJ or by HR. In contrast, Rad52 binding is a marker of the commitment of a break towards HR. Given these considerations, one would expect that the percentage of cells in the population displaying Tel1 foci exceeds that of Rad52. Yet, the kinetics, dose-dependency and percentages of both Rad52 and Tel1 foci formation were alike when using the Cas9 system or in response to zeocin (compare Fig 4E with 5A and Fig 5B with 5C), suggesting a major commitment of breaks in both systems towards HR. In the case of Cas9, the targeting of sequences sharing large homologies (Ty elements) may favor the use of HR for repair. Moreover, the long residence time of the Cas9 nuclease on one side of the cut after breaking (25) may obstruct NHEJ implementation. Similarly, bleomycins, a family to which zeocin belongs, are also suggested to block DSBs ends (39). Thus, while both in human and in *S. cerevisiae* cells NHEJ can achieve the repair of Cas9-induced breaks to different extents (40–44), our confrontation of Tel1 *versus* Rad52 data suggests a major contribution of HR in the face of these lesions in *S. cerevisiae*.

We exploited our system to compare the kinetics of damage sensing (Tel1), processing (Rfa1, revealing resection) and HR engagement (Rad52). Upon Cas9 induction, cleavage activity is persistent and, as fast as a break is repaired, it becomes available for cleavage again. Further, Tel1 foci on a given DSB disappear when resection takes place (30). Thus, only the

curve slope speaks of the foci formation kinetics before the dynamic equilibrium is reached. With this in mind, we first observed that the percentage of cells displaying Rfa1 foci is always double that of cells displaying Tel1 or Rad52 foci, suggesting that resection progresses comparatively for longer, thus increasing the residence time of Rfa1 bodies. We also observed that the kinetics of foci formation of all three proteins are very similar for a given number of cuts, indicating that the transition from one step to the next may take place very fast. Last, we acknowledged a fair dose-dependent response in the number of such foci. An exception concerns the x 15-cuts scenario, where Rfa1 foci formed in more cells, and Rad52 ones appeared faster, than when 59 cuts were induced. This may highlight the phenomenon of interference at clustered DSBs. Indeed, DSBs concentrated at near-by locations, as those induced in the x 59-cuts scenario, are less efficiently repaired than isolated lesions (45).

More than 13 proteins working in the cascade of DSB sensing and repair have been fluorescently labelled and their *in vivo* foci formation ability scored by microscopy (30,32,46). With the exception of post-Spo11 cutting during meiosis, with up to 15 Rad52 foci measured per cell (47), these proteins gather in a single focus irrespective of the number of DSBs. For example, even at doses as high as 160 krad, which induces up to 80 DSBs per cell, haploid *S. cerevisiae* cells as the ones used in this study eventually form a maximum of 2 Rad52 foci (47). Of all this set, the only protein openly reported to simultaneously form multiple nuclear foci is Rfa1, and these sites are identified as post-replicative repair territories (48). The difference in whether the factor gathers under a single focus or as multiple foci may come from the nature of the lesion to be repaired (a DSB *versus* a damaged but not broken template). Additionally, the DNA-binding properties of the factor under consideration may restrict its mobility. For example, Rfa1 remains bound to the DNA (49), perhaps preventing the nucleation of all breaks at a single location. An interesting finding of our study is the evidence that Tel1 can form multiple (up to 8) foci per cell in response to zeocin. So far, Tel1 is the only factor displaying such a behavior when DSBs inducing agents are used in haploid *S. cerevisiae*. This ability could relate to its role in sensing and not in processing. It may be that lesion recognition takes place where it happened or, at the most, the gathering process during recognition is restricted to the local environment. Later on, from the moment resection by nucleases takes place, the processing and the subsequent steps are ruled by different nucleation abilities. In support of these transitions, Tel1 foci were reported to colocalize neither with Rfa1 nor Rad52 ones (30),

and even subsequent downstream events, such as the processing of recombination intermediates by nucleases like Slx4 or Mus81, do not occupy the same space as Rad52 centers (32). This said, we noted that Tel1 formed only one focus in response to Cas9 nuclease expression, irrespective of the dose of induced DSBs. This may relate to Ty retrotransposons, which are targeted by Cas9 in our system, being clustered within a single nuclear subdomain (50).

Analysis of numerous nuclei photographed from distinct angles led us to propose that Tel1 foci form at the periphery of the nucleus, although not all over the sphere, but as a ring. Additional proximity analysis visualizing a fluorescently tagged nucleoporin in order to illuminate the nuclear periphery confirmed this notion. The fact that Tel1 foci form in close contact to the nuclear periphery raises the prospect that a nucleation factor presumably exists close to, or even at, the nuclear membrane that serves to scaffold them. Tel1 and the other DNA damage response apical kinase, Mec1, are Phosphatidyl Inositol 3-kinase-like kinases. Although these kinases are thought not to bear the ability to phosphorylate phosphatidylinositol (PI) moieties any longer (51), they may have kept their ability to bind such molecules. In agreement, the Mec1 human homolog, ATR, was reported to be assisted by phosphoinositides in order to correctly nucleate in the shape of foci upon DNA damage (48). Furthermore, ATR demonstrates ability to sense lipids at membranes (52), and to act at the nuclear membrane to phosphorylate its targets in response to mechanical cues (53). Therefore, it is very tempting to suggest that Tel1 is being guided at lipid hotspots at the inner nuclear membrane either to exert its DNA breaks sensing activity, or to engage downstream actions after having sensed them. In a further attempt to venture into this direction, we note the striking similarity of the Tel1 foci-defined ring and the discrete spots described along the nuclear-vacuole junction as marked by the Fatty Acids metabolism-related enzyme Mdm1 (54). It will be worth exploring in a near future whether Tel1 nucleation relates to the metabolism of lipids.

635

636 **Abbreviations:**

637 **CFP**, Cyan Fluorescent Protein; **CPT**, camptothecin; **CRISPR**, Clustered Regularly Interspaced Short Palindromic

638 Repeats; **DIC**, differential interference contrast; **DSBs**, Double Strand Breaks; **gRNA**, guide RiboNucleic Acid; **G$_1$**,

639 Gap 1 phase; **G$_2$**, Gap 2 phase; **HR**, Homologous Recombination; **NHEJ**, Non-Homologous End Joining; **PAM**,

640 protospacer adjacent motif; **PFGE**, pulsed field gel electrophoresis; **RFP**, red fluorescent protein; **S**, DNA synthesis

641 phase; **WT**, wild type; **yEGFP**, yeast Enhanced Green Fluorescent Protein; **YFP**, Yellow Fluorescent Protein; **YNB**,

642 yeast nitrogen base; **YEPD**, yeast extract peptone dextrose.

643

646

References

648 1. Rouse J, Jackson SP. Interfaces between the detection, signaling, and repair of DNA

649   damage. Science (80-). 2002;297(5581):547–51.

650 2. Pardo B, Gómez-González B, Aguilera A. DNA double-strand break repair: How to fix

651   a broken relationship. Cell Mol Life Sci. 2009;66(6):1039–56.

652 3. Stein A, Kalifa L, Sia EA. Members of the RAD52 Epistasis Group Contribute to

653   Mitochondrial Homologous Recombination and Double-Strand Break Repair in

654   Saccharomyces cerevisiae. PLoS Genet. 2015;11(11):1–20.

655 4. Iacovoni JS, Caron P, Lassadi I, Nicolas E, Massip L, Trouche D, et al. High-resolution

656   profiling of γh2AX around DNA double strand breaks in the mammalian genome.

657   EMBO J. 2010;29(8):1446–57.

658 5. Peritore M, Reusswig K, Bantele SCS, Straub T, Peritore M, Reusswig K, et al. Strand-

659   specific ChIP-seq at DNA breaks distinguishes ssDNA versus dsDNA binding and

660   refutes single-stranded nucleosomes Short Article Strand-specific ChIP-seq at DNA

661   breaks distinguishes ssDNA versus dsDNA binding and refutes single-stranded. Mol

662   Cell [Internet]. 2021;1–13. Available from: https://doi.org/10.1016/j.molcel.2021.02.005

663 6. Westmoreland JW, Summers JA, Holland CL, Resnick MA, Lewis LK. Blunt-ended

664   DNA double-strand breaks induced by endonucleases PvuII and EcoRV are poor

665   substrates for repair in Saccharomyces cerevisiae. DNA Repair (Amst) [Internet].

666   2010;9(6):617–26. Available from: http://dx.doi.org/10.1016/j.dnarep.2010.02.008

667 7. Lewis LK, Westmoreland JW, Resnick MA. Repair of endonuclease-induced double-

668   strand breaks in Saccharomyces cerevisiae: Essential role for genes associated with

669   nonhomologous end- joining. Genetics. 1999;152(4):1513–29.

670 8. Lewis LK, Kirchner JM, Resnick MA. Requirement for End-Joining and Checkpoint

671   Functions, but Not RAD52 -Mediated Recombination, after Eco RI Endonuclease

672   Cleavage of Saccharomyces cerevisiae DNA . Mol Cell Biol. 1998;18(4):1891–902.

673 9. Bellaiche Y, Mogila V, Perrimon N. I-SceI endonuclease, a new tool for studying DNA

674   double strand break repair mechanisms in Drosophila. Genetics. 1999;152(3):1037–44.

675 10. Rouet P, Smih F, Jasin M. Introduction of double-strand breaks into the genome of

676   mouse cells by expression of a rare-cutting endonuclease. Mol Cell Biol.

677   1994;14(12):8096–106.

678 11. Haber JE. A Life Investigating Pathways That Repair Broken Chromosomes. Annu

679   Rev Genet. 2016;50:1–28.

680 12. Plessis A, Perrin A, Habert JE, Dujon B. Site-specific Recombination Determined by I-

681   SceI, a Mitochondrial Group I Intron-Encoded Endonuclease Expressed in the Yeast

682   Nucleus. Genetics. 1992;130:451–60.

683 13. Choulika A, Perrin A, Dujon B, Nicolas JF. Induction of homologous recombination in

684   mammalian chromosomes by using the I-SceI system of Saccharomyces cerevisiae.

685   Mol Cell Biol. 1995;15(4):1968–73.

686 14. Gnügge R, Symington LS. Efficient DNA double-strand break formation at single or

687   multiple defined sites in the Saccharomyces cerevisiae genome. Nucleic Acids Res.

688   2020;48(20):1–10.

689 15. Llorente B, Symington LS. The Mre11 Nuclease Is Not Required for 5′ to 3′ Resection at

690   Multiple HO-Induced Double-Strand Breaks. Mol Cell Biol. 2004;24(21):9682–94.

691   16. Mantiero D, Clerici M, Lucchini G, Longhese MP. Dual role for Saccharomyces
692   cerevisiae Tel1 in the checkpoint response to double-strand breaks. EMBO Rep.
693   2007;8(4):380–7.

694   17. Wang R, Kamgoue A, Normand C, Léger-Silvestre I, Mangeat T, Gadal O. High
695   resolution microscopy reveals the nuclear shape of budding yeast during cell cycle
696   and in various biological states. J Cell Sci. 2016;129(24):4480–95.

697   18. Karanasios E, Barbosa AD, Sembongi H, Mari M, Han GS, Reggiori F, et al. Regulation
698   of lipid droplet and membrane biogenesis by the acidic tail of the phosphatidate
699   phosphatase Pah1p. Mol Biol Cell. 2013;

700   19. Tourrière H, Saksouk J, Lengronne A, Pasero P. Single-molecule Analysis of DNA
701   Replication Dynamics in Budding Yeast and Human Cells by DNA Combing. Bio-
702   Protocol. 2017;7(11):1–17.

703   20. Forstemann K, Hoss M, Lingner J. Telomerase-dependent repeat divergence at the 3′
704   ends of yeast telomeres. Nucleic Acids Res. 2000;28(14):2690–4.

705   21. Teixeira MT, Arneric M, Sperisen P, Lingner J. Telomere length homeostasis is
706   achieved via a switch between telomerase- extendible and -nonextendible states. Cell.
707   2004;117(3):323–35.

708   22. Mans R, Wijsman M, Daran-Lapujade P, Daran JM. A protocol for introduction of
709   multiple genetic modifications in Saccharomyces cerevisiae using CRISPR/Cas9. FEMS
710   Yeast Res. 2018;18(7):1–13.

711   23. Dicarlo JE, Norville JE, Mali P, Rios X, Aach J, Church GM. Genome engineering in
712   Saccharomyces cerevisiae using CRISPR-Cas systems. Nucleic Acids Res.
713   2013;41(7):4336–43.

714   24. Sheff MA, Thorn KS. Optimized cassettes for fluorescent protein tagging in
715   Saccharomyces cerevisiae. Yeast. 2004;21(8):661–70.

716   25. Sternberg SH, Redding S, Jinek M, Greene EC, Doudna JA. DNA interrogation by the
717   CRISPR RNA-guided endonuclease Cas9. Nature. 2014;507(7490):62–7.

718   26. Kim JM, Vanguri S, Boeke JD, Gabriel A, Voytas DF. Transposable elements and
719   genome organization: A comprehensive survey of retrotransposons revealed by the
720   complete Saccharomyces cerevisiae genome sequence. Genome Res. 1998;8(5):464–78.

721   27. Fleiss A, O'Donnell S, Fournier T, Lu W, Agier N, Delmas S, et al. Reshuffling yeast

722   chromosomes with CRISPR Cas9. PLoS Genet. 2019;15(8):1–26.

723   28.   Matheson K, Parsons L, Gammie A. Whole-genome sequence and variant analysis of

724   W303, a widely-used strain of Saccharomyces cerevisiae. G3 Genes, Genomes, Genet.

725   2017;7(7):2219–26.

726   29.   Weinert TA, Hartwell LH. The RAD9 gene controls the cell cycle response to DNA

727   damage in saccharomyces cerevisiae. Science (80-). 1988;241(4863):317–22.

728   30.   Lisby M, Barlow JH, Burgess RC, Rothstein R. Choreography of the DNA damage

729   response: Spatiotemporal relationships among checkpoint and repair proteins. Cell.

730   2004;118(6):699–713.

731   31.   Lisby M, Mortensen UH, Rothstein R. Colocalization of multiple DNA double-strand

732   breaks at a single Rad52 repair center. Nat Cell Biol. 2003;5(6):572–7.

733   32.   Saugar I, Jiménez-Martín A, Tercero JA. Subnuclear Relocalization of Structure-

734   Specific Endonucleases in Response to DNA Damage. Cell Rep. 2017;20(7):1553–62.

735   33.   Bernstein KA, Mimitou EP, Mihalevic MJ, Chen H, Sunjaveric I, Symington LS, et al.

736   Resection activity of the Sgs1 helicase alters the affinity of DNA ends for homologous

737   recombination proteins in Saccharomyces cerevisiae. Genetics. 2013;195(4):1241–51.

738   34.   Menin L, Ursich S, Trovesi C, Zellweger R, Lopes M, Longhese MP, et al. Tel1/ ATM

739   prevents degradation of replication forks that reverse after topoisomerase poisoning .

740   EMBO Rep. 2018;19(7):1–13.

741   35.   Nakada D, Matsumoto K, Sugimoto K. ATM-related Tel1 associates with double-

742   strand breaks through an Xrs2-dependent mechanism. Genes Dev. 2003;17(16):1957–

743   62.

744   36.   Clerici M, Baldo V, Mantiero D, Lottersberger F, Lucchini G, Longhese MP. A

745   Tel1/MRX-Dependent Checkpoint Inhibits the Metaphase-to-Anaphase Transition

746   after UV Irradiation in the Absence of Mec1. Mol Cell Biol. 2004;24(23):10126–44.

747   37.   Hirano Y, Fukunaga K, Sugimoto K. Rif1 and Rif2 Inhibit Localization of Tel1 to DNA

748   Ends. Mol Cell [Internet]. 2009;33(3):312–22. Available from:

749   http://dx.doi.org/10.1016/j.molcel.2008.12.027

750   38.   Krol K, Brozda I, Skoneczny M, Bretne M, Skoneczna A. A genomic screen revealing

751   the importance of vesicular trafficking pathways in genome maintenance and

752   protection against genotoxic stress in diploid saccharomyces cerevisiae cells. PLoS

753   One. 2015;10(3):1–32.

754   39.   Tam ATY, Pike BL, Hammet A, Heierhorst J. Telomere-related functions of yeast KU
755   in the repair of bleomycin-induced DNA damage. Biochem Biophys Res Commun.
756   2007;357(3):800–3.

757   40.   Lemos BR, Kaplan AC, Bae JE, Ferrazzoli AE, Kuo J, Anand RP, et al. CRISPR/Cas9
758   cleavages in budding yeast reveal templated insertions and strand-specific
759   insertion/deletion profiles. Proc Natl Acad Sci U S A. 2018;115(9):E2010–47.

760   41.   Román-Rodríguez FJ, Ugalde L, Álvarez L, Díez B, Ramírez MJ, Risueño C, et al.
761   NHEJ-Mediated Repair of CRISPR-Cas9-Induced DNA Breaks Efficiently Corrects
762   Mutations in HSPCs from Patients with Fanconi Anemia. Cell Stem Cell.
763   2019;25(5):607-621.e7.

764   42.   van Overbeek M, Capurso D, Carter MM, Thompson MS, Frias E, Russ C, et al. DNA
765   Repair Profiling Reveals Nonrandom Outcomes at Cas9-Mediated Breaks. Mol Cell
766   [Internet]. 2016;63(4):633–46. Available from:
767   http://dx.doi.org/10.1016/j.molcel.2016.06.037

768   43.   Tran NT, Bashir S, Li X, Rossius J, Chu VT, Rajewsky K, et al. With homologous
769   recombination factors. Front Genet. 2019;10(APR):1–13.

770   44.   Jayavaradhan R, Pillis DM, Goodman M, Zhang F, Zhang Y, Andreassen PR, et al.
771   CRISPR-Cas9 fusion to dominant-negative 53BP1 enhances HDR and inhibits NHEJ
772   specifically at Cas9 target sites. Nat Commun [Internet]. 2019;10(1):1–13. Available
773   from: http://dx.doi.org/10.1038/s41467-019-10735-7

774   45.   Nickoloff JA, Sharma N, Taylor L. Clustered DNA double-strand breaks: Biological
775   effects and relevance to cancer radiotherapy. Genes (Basel). 2020;11(1).

776   46.   Chen H, Lisby M, Symington LS. RPA Coordinates DNA End Resection and Prevents
777   Formation of DNA Hairpins. Mol Cell [Internet]. 2013;50(4):589–600. Available from:
778   http://dx.doi.org/10.1016/j.molcel.2013.04.032

779   47.   Lisby M, Rothstein R, Mortensen UH. Rad52 forms DNA repair and recombination
780   centers during S phase. Proc Natl Acad Sci U S A. 2001;98(15):8276–82.

781   48.   Wong RP, García-Rodríguez N, Zilio N, Hanulová M, Ulrich HD. Processing of DNA
782   Polymerase-Blocking Lesions during Genome Replication Is Spatially and Temporally
783   Segregated from Replication Forks. Mol Cell. 2020;77(1):3-16.e4.

784   49.   Miné-Hattab J, Heltberg M, Villemeur M, Guedj C, Mora T, Walczak AM, et al. Single

785   molecule microscopy reveals key physical features of repair foci in living cells. Elife.

786   2021;10:1–29.

787   50.   O'Sullivan J. M., Sontam D. M., Grierson R. and Jones B. Repeated elements

788   coordinate the spatial organization of the yeast genome. Yeast. 2009;26:125–38.

789   51.   Bradbury JM, Jackson SP. ATM and ATR. Curr Biol. 2003;13(12):468.

790   52.   Zhang XH, Zhao C, Ma ZA. The increase of cell-membranous phosphatidylcholines

791   containing polyunsaturated fatty acid residues induces phosphorylation of p53

792   through activation of ATR. J Cell Sci. 2007;120(23):4134–43.

793   53.   Kumar A, Mazzanti M, Mistrik M, Kosar M, Beznoussenko G V., Mironov AA, et al.

794   ATR mediates a checkpoint at the nuclear envelope in response to mechanical stress.

795   Cell. 2014;158(3):633–46.

796   54.   Hariri H, Rogers S, Ugrankar R, Liu YL, Feathers JR, Henne WM. Lipid droplet

797   biogenesis is spatially coordinated at ER –vacuole contacts under nutritional stress .

798   EMBO Rep. 2018;19(1):57–72.

799

800

Supporting Information
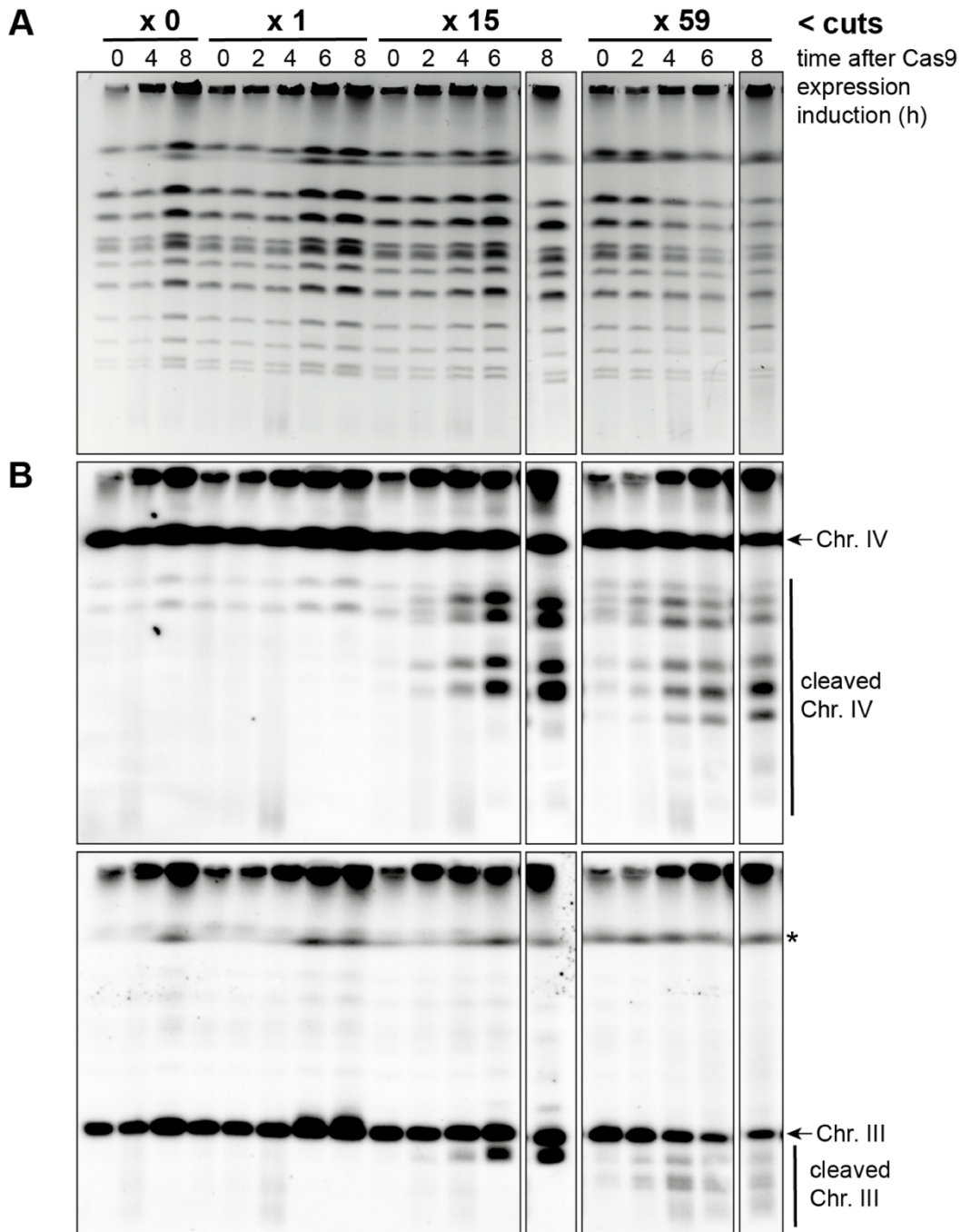
S1 Fig. PFGE used for restriction analyses of chromosome cleavage by Cas9

A. PFGE was prepared and run as in **Fig 2B**, and stained with ethidium bromide. Please note that the time point 8 h for the x 15- and x 59-cuts were inadvertently exchanged during gel loading. As such, the broken boxes indicate that the two lanes have now been replaced where they belong.

808   **B.** Southern blot hybridizations against chromosome (Chr.) IV (top) and III (bottom) against

809   the DNA run in **(A)**. The asterisk denotes a residual band after incomplete stripping of

810   chromosome IV hybridization.

811
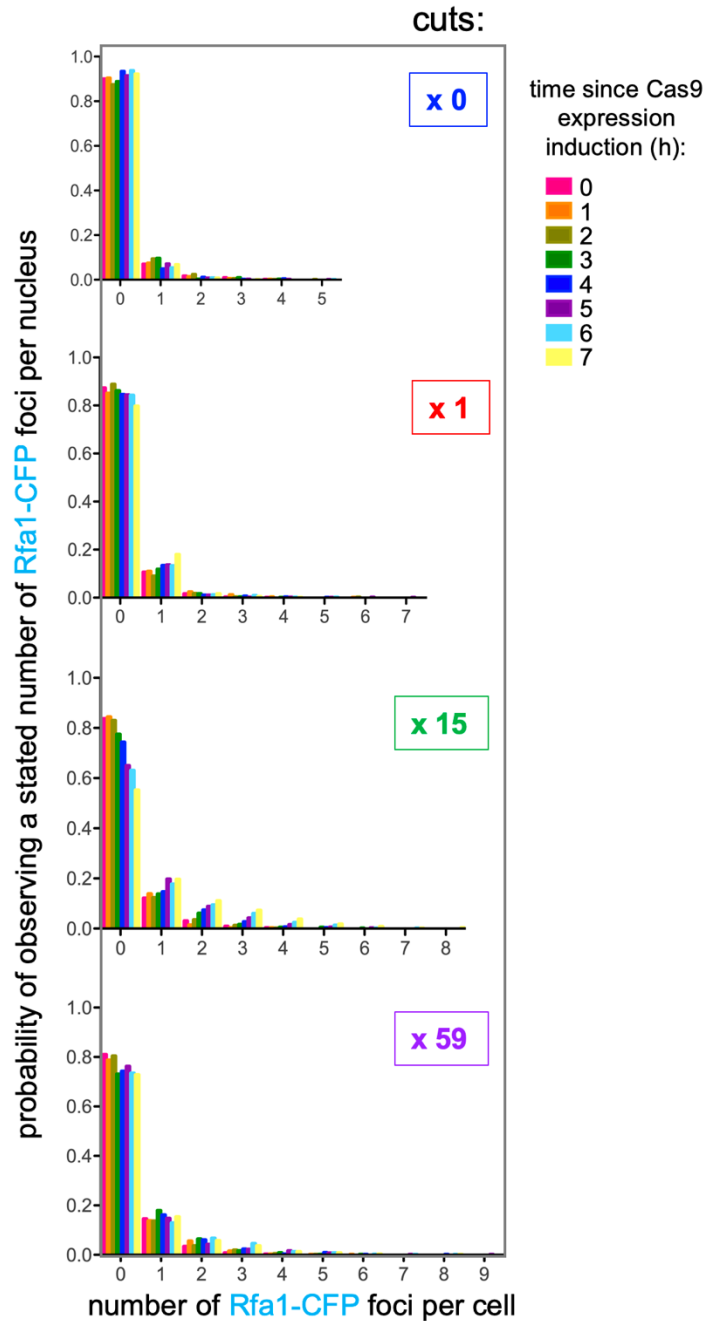
812

813   **S2 Fig. Quantification of the number of Rfa1-CFP foci per nucleus in response to Cas9 cuts**

814   Graphs showing the probability distribution of finding a stated number of Rfa1-CFP foci in a

815   given nucleus at a given time as calculated from the experiments presented in Fig 4D. The

816   probability distribution is calculated upon merging the three experiments presented in Fig 4D.

817   All three independent experiments had a similar profile. At least 200 cells were counted per

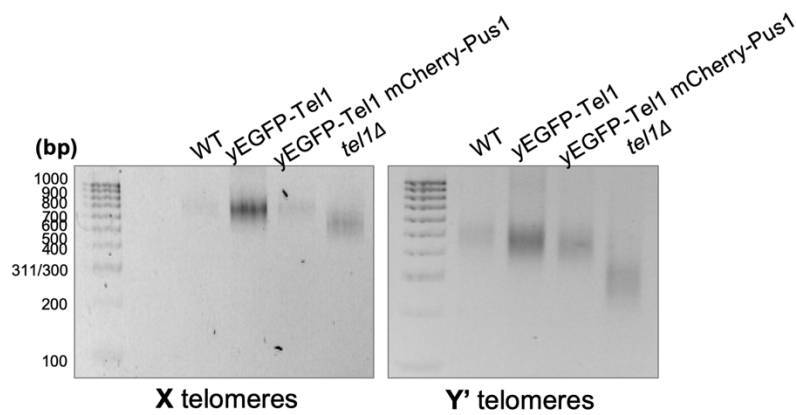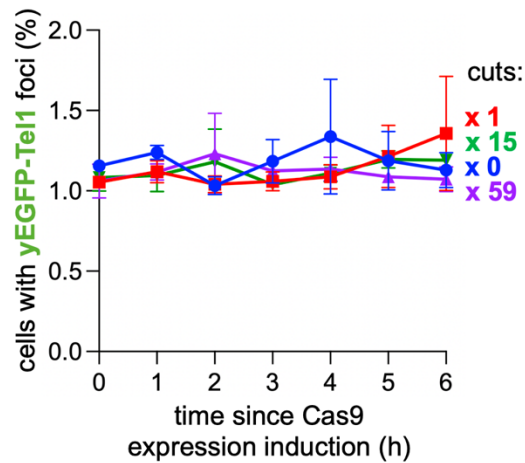818   time-point, condition and experiment.

819

820
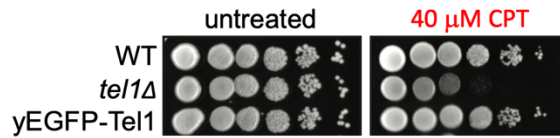
821

822   **S3 Fig. Controls ensuring that the yEGFP-Tel1-tagged strain behaves as a WT**

823   **A.** 10-fold serial dilutions of *S. cerevisiae* cells of the indicated genotypes spotted onto YPED

824   rich medium plates supplemented either with DMSO (untreated) or with 40 µM CPT,

825   incubated 2 to 3 days at 26°C and imaged.

826   **B.** Telomeres (X and Y') length was measured by PCR-mediated amplification (see M&M) from

827   genomic DNA extracted from the indicated strains. *tel1Δ* cells were included as a control for

828   their telomere shortening phenotype. yEGFP-Tel1 cells, whether additionally bearing

829   mCherry-Pus1 or not, display WT-length telomeres.

830   **C.** The mean number of Tel1 foci per cell (as established by counting the total number of foci

831   divided by the total number of cells) was calculated out of at least 150 cells for each time point

832   and condition. This experiment was done three times, and the plotted value is the mean out of

833   those three experiments. The error bars correspond to the standard error of the mean associ-

834   ated to them.